Raman Lidar (RL) Handbook

November 2004

D. D. Turner

Work supported by the U.S. Department of Energy,
Office of Science, Office of Biological and Environmental Research

Contents

Figures

1. General Overview

The Raman Lidar (RL) is an active, ground-based laser remote sensing instrument that measures vertical profiles of water-vapor mixing ratio and several cloud- and aerosol-related quantities. Lidar (light detection and ranging) is the optical analog of radar, using pulses of laser radiation to probe the atmosphere. This system is fully computer automated, and will run unattended for many days following a brief (~5-minute) startup period. The self-contained system (requiring only external electrical power) is housed in a climate-controlled 8'x8'x20' standard shipping container.

2. Contacts

2.1 Mentor

Tim Tooman
Sandia National Laboratories
P.O. Box 969, MS 9056
Livermore, CA 94551-0969
Phone: 510-294-2752
Fax: 510-294-1559
tooman@sandia.gov

John Goldsmith (engineering)
Sandia National Laboratories
Phone: 925-294-2432
jgold@sandia.gov

2.2 Instrument Developer

John Goldsmith
Sandia National Laboratories
P.O. Box 969, MS 9409
Livermore, CA 94551-0969
Phone: 510-294-2432
Fax: 510-294-3870
jgold@sandia.gov

3. Deployment Locations and History

The Raman lidar is currently operational at the Southern Great Plains CART site. The system generally is not operated during periods of low cloud base or precipitation. Pending installation of a hail shield, it is only operated when personnel are present at the site (continuously during intensive observational periods, normal week-day working hours otherwise).

4. Near-Real-Time Data Plots

Near realtime quicklooks.

5. Data Description and Examples

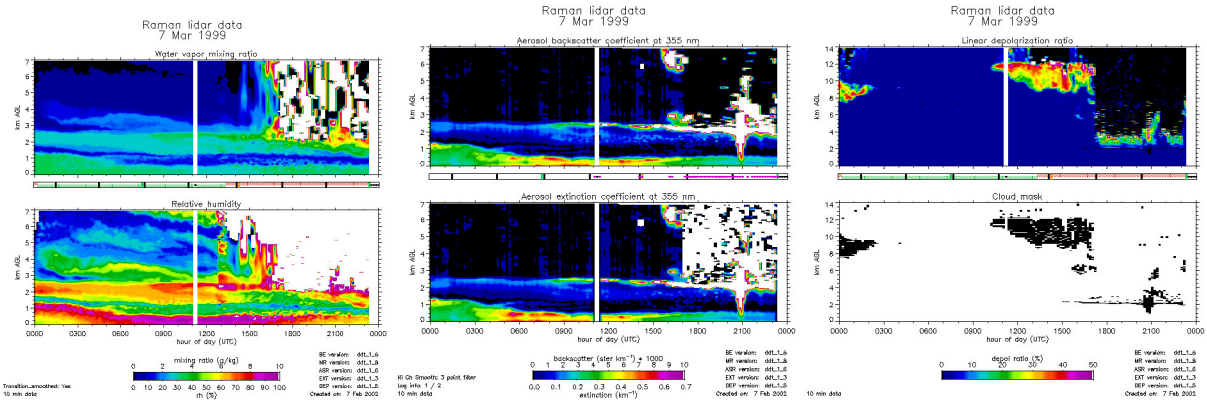

Figure 1.

Additional examples of measurements taken during the September 1996 Water Vapor Intensive Observational Period are presented in Figure 1. These examples are PRELIMINARY, pending final analysis using calibration constants determined from the final analysis of all IOP data.

Nighttime Water Vapor Image

The performance of Raman lidar systems is best during nighttime, in the absence of the daytime solar background. The nighttime false-color image (PDF document or gif image) illustrates the temporal and spatial resolution provided by Raman lidar. The time axis is in "universal time" (GMT); the local time for the measurement started at 7:00 pm on September 27, through approximately 8:30 am on September 28. The altitude axis is km AGL (above ground level). This image consists of "pixels" 39 m "high" by 2 minutes "wide," with color representing the water-vapor mixing ratio. The vertical stripes at ~1:00 UT are caused by clouds at ~2 km AGL (the laser beam cannot penetrate optically thick clouds; hence the ratio of water vapor to nitrogen signal is ~0/0, producing "noise"). The speckled appearance after ~12:30 UT is due to the increasing solar background as the sun rises.

Nighttime Raman Lidar - Radiosonde Comparison

One method for examining the performance of Raman lidar systems is to compare water-vapor profiles with measurements from collocated radiosondes; many such measurements were made during the water-vapor IOP. One nighttime example is shown in this plot (PDF document or gif image) (11:28 UT on September 28, or 6:28 am local time). This plot shows a 5-minute average of the Raman lidar data, with vertical resolution varying from 39 m at lower altitudes to 312 m at higher altitudes (the variation in vertical resolution with altitude can be determined by the vertical spacing of the error bars). This plot is displayed with a logarithmic x-axis to illustrate the nighttime capabilities of the Raman lidar for measuring upper-tropospheric water vapor; longer temporal averages and decreased vertical resolution can reduce the statistical errors still further. Discrepancies between the two profiles may be due to measurement errors, but are more likely due to the fact that the radiosonde blows downwind as it rises, and thus the vertical-pointing lidar and the radiosonde do not measure the same air parcels.

Daytime Water Vapor Image

The CART Raman lidar has state-of-the-art daytime capabilities also. A sample daytime false-color image (PDF document or gif image) illustrates this capability. In this image, the "pixels" are 10 minutes "wide," with "height" varying from 78 m near the ground to 312 m at higher altitudes. This image does not have the resolution or altitude range of the nighttime image simply due to the difficulty of extracting the relatively weak Raman lidar signal from the large solar background.

Daytime Raman Lidar - Radiosonde Comparison

A daytime comparison with a radiosonde is shown in this plot (PDF document or gif image) (17:30 UT on September 21, 12:30 pm local time). The Raman lidar measurement represents a 10-minute average, with vertical resolution varying from 78 m near the ground to 312 m at higher altitudes. Again, the daytime performance cannot match the nighttime performance, but this figure illustrates the capabilities of the system for measuring the majority of tropospheric moisture even during mid-day.

24-Hour Water Vapor Image

The Raman lidar automatically switches between "daytime" and "nighttime" operation simply by adding or removing neutral density filters in the water-vapor detection channels. The system thus provides continuous, uninterrupted multiple-day coverage; a Raman lidar capability that we believe is unique to this instrument. A false-color image (PDF document or gif image) from measurements recorded on September 10 illustrates this 24-hour capability.

Weather System (Water Vapor, Aerosol, and Depolarization Images)

An interesting weather system passed over the CART site on September 20, with a variety of cloud types and associated virga. Water-vapor PDF document or gif image), aerosol scattering ratio (PDF document or gif image), and depolarization (PDF document or gif image) images are shown for the period 17:00-24:00 UT (12:00 pm - 7:00 pm local time). In the water-vapor image, the white regions above ~3.5 km are "noise" caused by the laser beam being block by clouds. Comparing the aerosol scattering and depolarization images, it is interesting to note the very low (~0%) depolarization values below ~3.5 km beneath several of the clouds (the background depolarization value of ~0.7% is caused by slight depolarization from Rayleight and rotational Raman scattering). This decrease in depolarization is caused by melting of the cloud ice particles as they descend; the resulting liquid droplets are spherical, producing significant scattering (evident in the aerosol scattering image) with essentially no depolarization.

Narrow and Wide Field-of-View Channel Comparison

The narrow and wide field-of-view channels provide two nearly independent detection systems for exploring potential systematic effects in the lidar system (the common telescope being the only common element). Water-vapor "images" produced with the two can be used to visually compare measurements made with the two channels. The figure (PDF document or gif image) displays such a comparison for the nighttime period ~1:30-13:30 UT on October 5 (~8:30 pm October 4 to ~8:30 am October 5, local time), just after the end of the water-vapor IOP. The similarity of the two images is striking. Close examination

illustrates the better performance of the "low channel" at lower altitudes and the "high channel" at higher altitudes, the reason for having the two channels in the first place.

5.1 Data File Contents

5.1.1 Primary Variables and Expected Uncertainty

The Raman Lidar has independent measurement channels that record range-resolved backscatter signals from molecular water vapor, molecular nitrogen, and combined Rayleigh and aerosol contributions (the latter at polarizations parallel and perpendicular to the polarization of the laser beam). Primary quantities obtained from these backscatter signals are range-resolved vertical profiles of water-vapor mixing ratio (g/kg), aerosol scattering ratio (unitless), and backscatter depolarization ratio (percent). Additional cloud- and aerosol-related measurements can also be derived from the backscatter signals.

5.1.1.1 Definition of Uncertainty

All "raw" signals are simply photon counts for the specified averaging interval (in time and range). Poisson statistics can therefore be used to calculate statistical uncertainties (error bars) for derived quantities. Potential systematic errors appear to be smaller than statistical errors, but are being explored carefully.

5.1.2 Secondary/Underlying Variables

This section is not applicable to this instrument.

5.1.3 Diagnostic Variables

This section is not applicable to this instrument.

5.1.4 Data Quality Flags

RL Data Object Design Changes for ARM netCDF file header descriptions.

5.1.5 Dimension Variables

This section is not applicable to this instrument.

5.2 Annotated Examples

This section is not applicable to this instrument.

5.3 User Notes and Known Problems

This section is not applicable to this instrument.

5.4 Frequently Asked Questions

This section is not applicable to this instrument.

6. Data Quality

6.1 Data Quality Health and Status

The following links go to current data quality health and status results.

- DQ HandS (Data Quality Health and Status)
- NCVweb for interactive data plotting using.

The tables and graphs shown contain the techniques used by ARM's data quality analysts, instrument mentors, and site scientists to monitor and diagnose data quality.

6.2 Data Reviews by Instrument Mentor

Some QC products for the Raman Lidar have been developed by Dave Turner. Among other things, they compare the output to other relevant instruments, such as sondes. These products appear to be sufficient for the moment, at least until we have more experience with the instrument.

6.3 Data Assessments by Site Scientist/Data Quality Office

All DQ Office and most Site Scientist techniques for checking have been incorporated within DQ HandS and can be viewed there.

6.4 Value-Added Procedures and Quality Measurement Experiments

Many of the scientific needs of the ARM Program are met through the analysis and processing of existing data products into "value-added" products or VAPs. Despite extensive instrumentation deployed at the ARM CART sites, there will always be quantities of interest that are either impractical or impossible to measure directly or routinely. Physical models using ARM instrument data as inputs are implemented as VAPs and can help fill some of the unmet measurement needs of the program. Conversely, ARM produces some VAPs not in order to fill unmet measurement needs, but instead to improve the quality of existing measurements. In addition, when more than one measurement is available, ARM also produces "best estimate" VAPs. A special class of VAP called a Quality Measurement Experiment (QME) does not output geophysical parameters of scientific interest. Rather, a QME adds value to the input datastreams by providing for continuous assessment of the quality of the input data based on internal consistency checks, comparisons between independent similar measurements, or comparisons between measurement with modeled results, and so forth. For more information, see the VAPs and QMEs web page.

7. Instrument Details

7.1 Detailed Description

7.1.1 List of Components

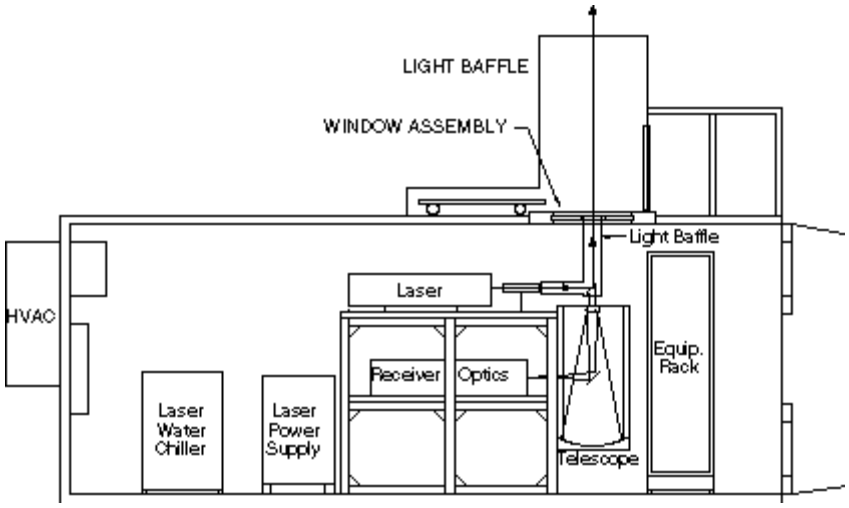

Figure 2.

The CART Raman Lidar is a custom instrument developed for the ARM program by Sandia National Laboratories. This diagram in Figure 2 shows the layout of the system inside the shipping container; a diagram of the receiver optics appears in the next section of this page. Major commercially supplied subcomponents include:

- System enclosure (including optical mounting system, window/hatch assembly, climate control, and utilities): produced by Orca Photonic Systems, Inc.
- Laser: Continuum Model 9030 frequency-tripled Nd:YAG laser (30 Hz, 400 mJ pulses at 355 nm)
- Laser beam expander: 15x unit produced by CVI, Inc.
- Receiving telescope: 61 cm diameter f/9.3 Dall-Kirkham system produced by Optical Guidance Systems
- Dichroic beam splitters and narrow band interference filters: produced by Barr Associates
- Computer-controlled filter wheels: produced by CVI, Inc.
- Dichroic beam splitters and narrow band interference filters: produced by Barr Associates
- Photo multipliers: Thorn EMI Electron Tubes Model 9954B
- Amplifiers: Phillips Scientific Model 6950
- Discriminators: Phillips Scientific Model 6904
- Multichannel scalers: Santa Fe Energy Research Model MCS-100
- Data acquisition environment: National Instruments LabVIEW 3.1.

7.1.2 System Configuration and Measurement Methods

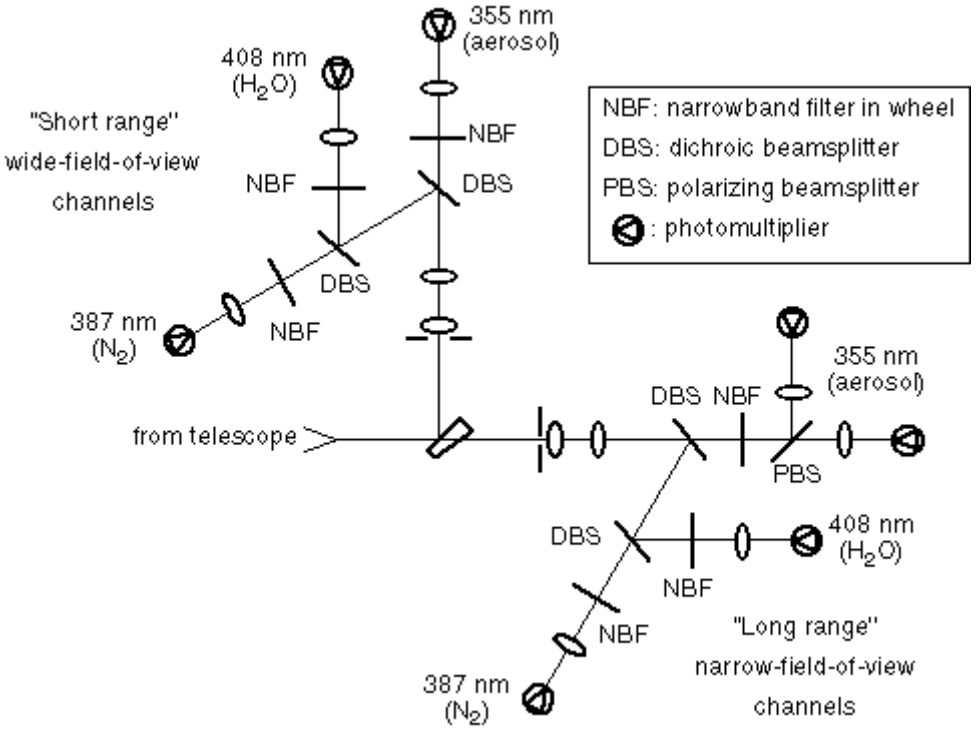

Figure 3.

The system's "receiver optics" that follow the telescope in the optical path are shown in Figure 3 (detailed characteristics appear in the table in the "Description of Observational Specifications" section below). Light collected by the telescope is first split into two pieces by a wedged beam splitter, with 10% directed into the "short-range" wide-field-of-view channels, and 90% into the "long-range" narrow-field-of-view channels. For each set of channels, the light first encounters an aperture (field stop), and is then collimated by field and collimating lenses. Dichroic beam splitters separate the light by wavelength into signals produced by backscatter from water vapor (408 nm), nitrogen (387 nm), and aerosol/Rayleigh scattering (355 nm, the laser wavelength), followed by narrow band interference filters, imaging lenses, and photo multipliers for each wavelength. In the "long-range" optics, a polarizing beam splitter is used to separately analyze the parallel and perpendicular polarization (relative to the laser beam) of the aerosol/Rayleigh scattering.

For system calibration purposes, computer-controlled filter wheels are used to replace the water-vapor and aerosol/Rayleigh filters by nitrogen filters. Signals recorded in this configuration can by used to determine any differences in the range dependence of the signals in the various channels, and to track the long-term relative sensitivity of the channels. During the daytime, the filter wheels add neutral-density filters to the water-vapor channels to prevent these high-sensitivity channels from being "swamped" by the large solar background. Neutral-density filters can also be added to the optical path for use in determining resolving time corrections (pulse-pileup effects) for the electronics in the photon-counting multichannel scaler electronics.

7.1.3 Specifications

Transmitter		Receiver	
Wavelength	355 nm	Diameter	61 cm
Laser	Nd:YAG third harmonic	Channel bandpass	0.3 nm (narrow fov) 1.2 nm (wide fov)
Energy/pulse	400 mJ	Filter transmission	30-40%
Repetition rate	30 Hz	Field of view	Dual, adjustable (typically 0.3 mr, 2 mr)
Beam Diameter	13 cm (~0.1 mr divergence)	Species	Rayleigh/aerosol (355 nm) Aerosol depol. (355 nm) Water vapor (408 nm) Nitrogen (387 nm)
Bandwidth	~2 cm^{-1}	Electronics	Photon counting 39 m range resolution

Figure 4.

The table in Figure 4 lists the system specifications. The finest vertical resolution is 39 m, determined by the minimum bin time of the photon-counting electronics. The nominal temporal resolution is one minute, although measurement periods as short as 10-30 seconds are possible. Because the system literally counts photons in equal-sized spatial and temporal bins, information is always recorded with 39-m vertical and (nominal) one-minute temporal resolution. However, during post-acquisition signal processing, additional averaging can be performed to trade off spatial and/or temporal resolution for improved sensitivity. In particular, this makes it possible to take advantage of the slower (in time and in space) variation of water vapor at higher altitudes to obtain higher sensitivity by post-acquisition averaging, while still having the high-resolution measurements at lower altitude.

7.2 Theory of Operation

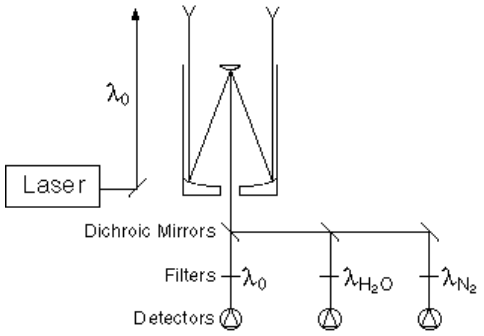

$$S_i(z) = \frac{k_i}{z^2} O(z)\, \sigma_i(\pi)\, n_i(z)\, q(\lambda_0, z)\, q(\lambda_i, z)$$

$$\text{Water-Vapor Mixing Ratio} \propto \frac{S_{H_2O}}{S_{N_2}}$$

$$\text{Aerosol Backscatter Ratio} \propto \frac{S_0}{S_{N_2}}$$

Figure 5.

Raman lidar systems detect selected species by monitoring the wavelength-shifted molecular return produced by vibrational Raman scattering from the chosen molecule or molecules, as illustrated in Figure 5. Narrow band, narrow field-of-view operation provides good daytime performance (discrimination of the weak Raman backscatter signal above the background daylight) without sacrificing nighttime performance. The system has been implemented as a dual field-of-view instrument because narrow field-of-view operation provides very weak short-range signals. A set of "wide" field-of-view channels provides better results for short-range signals (out to ~500 m for water vapor).

For each channel "i," the signal as a function of range z is inversely proportional to the range squared, and proportional to the product of constant k, overlap function O(z), Raman cross-section sigma(180 degree backscatter), number density n(z), attenuation of the laser beam traveling to the region of interest q(laser wavelength, z), and attenuation of the backscattered radiation q(backscatter wavelength, z).

By taking the ratio of the signal at the water-vapor wavelength to the signal at the nitrogen wavelength, most of the range-dependent terms drop out, and one is left with a quantity that is almost directly proportional to the water-vapor mixing ratio expressed as grams of water vapor per kilogram of dry air (a small correction for the wavelength dependence of the second attenuation term is easily taken into account). Similarly, by taking the ratio of the signal at the laser wavelength to the signal at the nitrogen wavelength, one is left with the aerosol backscatter ratio; this ratio is normalized such that it is unity in "clean air" (laser-wavelength scatter caused only by Rayleigh scattering), and is in excess of unity for scattering by parcels of air that contain aerosols (including cloud droplets/particles). Finally, analysis of the polarization dependence of the backscatter signal at the laser wavelength provides information on particle shape (phase); spherical particles (cloud droplets) do not depolarize the laser backscatter, whereas nonspherical particles (such as ice crystals in cirrus clouds) can significantly depolarize the laser backscatter.

7.3 Calibration

7.3.1 Theory

The primary calibration issue for the Raman lidar is determining the "proportionality constants" for the bottom two equations in the figure at the top of the Theory of Operations" section (and a similar one for depolarization). For each observable, a single constant must be determined for use over the entire vertical profile. For water vapor, three general approaches can be taken: 1) match entire profiles to other instruments that measure vertical profiles (e.g., radiosondes); 2) match profiles at a single altitude using a fixed-height in-situ sensor (e.g., a tower sensor); or 3) integrate profiles and match the precipitable water vapor with values derived from other instruments (e.g., microwave radiometer or GPS instrument). All three approaches are being used for the CART Raman lidar. The other observables are more straightforward. For the aerosol backscatter ratio, the calibration can be accomplished by examining a variety of profiles and finding a region of "clean" (aerosol-free) air, and then choosing the constant that makes the ratio unity in that region. For depolarization, daylight backgrounds from overcast days provide unpolarized light for calibration purposes.

7.3.2 Procedures

This section is not applicable to this instrument.

7.3.3 History

The initial instrument calibration was performed using the dataset from the first Water Vapor Intensive Observational Period (September 1996). A QME that compares Raman lidar water-vapor profiles to measurements obtained using other CART instruments is being used to investigate the stability of the calibration over time.

7.4 Operation and Maintenance

7.4.1 User Manual

This section is not applicable to this instrument.

7.4.2 Routine and Corrective Maintenance Documentation

This section is not applicable to this instrument.

7.4.3 Software Documentation

ARM netCDF file header descriptions may be found at RL Data Object Design Changes.

7.4.4 Additional Documentation

This section is not applicable to this instrument.

7.5 Glossary

See the ARM Glossary.

7.6 Acronyms

CART: Cloud and Radiation Testbed
Lidar: Light Detection and Ranging
IOP: Intensive Observational Period
PDF: Portable Document Format

Also see the ARM Acronyms and Abbreviations.

7.7 Citable References

Goldsmith, J.E.M., F.H. Blair, S.E. Bisson, and D.D. Turner. 1998. Turn-key Raman lidar for profiling atmospheric water vapor, clouds, and aerosols. *Applied Optics*, Volume 37, Number 21, pages 4979-4990.

For additional information on the Raman lidar technique, see Whiteman, D.N., S.H. Melfi, and R.A. Ferrare. 1992. Raman lidar system for the measurement of water vapor and aerosols in the Earth's atmosphere. *Applied Optics*, Volume 31, Number 16, pages 3068-3082.

Turner, D.D., and J.E.M. Goldsmith. 1999. Twenty-four-hour Raman lidar water vapor measurements during the Atmospheric Radiation Measurement Program's 1996 and 1997 water vapor intensive observation periods. *J. Atmos. Oceanic Technol.*, 16, 1062-1076.

Turner, D.D., W.F. Feltz, and R.A. Ferrare. 2000. Continuous water vapor profiles from operational active and passive remote sensors. *Bull. Amer. Meteor. Soc.*, 81, 1301-1317.